

# Gram-positive DsbE Proteins Function Differently from Gram-negative DsbE Homologs

A STRUCTURE TO FUNCTION ANALYSIS OF DsbE FROM *MYCOBACTERIUM TUBERCULOSIS*\*

Received for publication, October 29, 2003

Published, JBC Papers in Press, November 3, 2003, DOI 10.1074/jbc.M311833200

Celia W. Goulding<sup>‡</sup>, Marcin I. Apostol<sup>‡</sup>, Stefan Gleiter<sup>§</sup>¶, Angineh Parseghian<sup>||</sup>,  
James Bardwell<sup>§\*\*</sup>, Marila Gennaro<sup>‡‡</sup>, and David Eisenberg<sup>‡||§§</sup>

From the <sup>‡</sup>Howard Hughes Medical Institute and UCLA-Department of Energy Institute of Genomics and Proteomics, Los Angeles, California 90095-1570, the <sup>||</sup>Department of Chemistry and Biochemistry, UCLA, Los Angeles, California 90095-1570, the <sup>§</sup>Department of Molecular Cellular and Development Biology, University of Michigan, Ann Arbor, Michigan 48109-1048, and the <sup>‡‡</sup>Public Health Research Institute, Newark, New Jersey 07103

*Mycobacterium tuberculosis*, a Gram-positive bacterium, encodes a secreted Dsb-like protein annotated as *Mtb* DsbE (Rv2878c, also known as MPT53). Because Dsb proteins in *Escherichia coli* and other bacteria seem to catalyze proper folding during protein secretion and because folding of secreted proteins is thought to be coupled to disulfide oxidoreduction, the function of *Mtb* DsbE may be to ensure that secreted proteins are in their correctly folded states. We have determined the crystal structure of *Mtb* DsbE to 1.1 Å resolution, which reveals a thioredoxin-like domain with a typical CXXC active site. These cysteines are in their reduced state. Biochemical characterization of *Mtb* DsbE reveals that this disulfide oxidoreductase is an oxidant, unlike Gram-negative bacteria DsbE proteins, which have been shown to be weak reductants. In addition, the pK<sub>a</sub> value of the active site, solvent-exposed cysteine is ~2 pH units lower than that of Gram-negative DsbE homologs. Finally, the reduced form of *Mtb* DsbE is more stable than the oxidized form, and *Mtb* DsbE is able to oxidatively fold hirudin. Structural and biochemical analysis implies that *Mtb* DsbE functions differently from Gram-negative DsbE homologs, and we discuss its possible functional role in the bacterium.

Protein disulfide bonds are often buried and serve to stabilize protein structures. However, partially exposed disulfide bonds in the active sites of protein-disulfide oxidoreductases have a variety of mechanistic roles in protein folding, electron transport, and bioenergetics in organisms ranging from prokaryotes to humans. Most disulfide oxidoreductases contain a conserved thioredoxin-like domain such as in thioredoxin, eu-

karyotic protein disulfide bond isomerase, glutaredoxin (1), peroxiredoxins (2), and disulfide bond-forming proteins (Dsb).<sup>1</sup> Except for peroxiredoxins, all of these proteins share a common sequence motif (CXXC) at their active sites.

One such family of disulfide oxidoreductases is the Dsb proteins, which are best characterized in *Escherichia coli*. These proteins reside in the periplasmic space of Gram-negative bacteria (Fig. 1a) and are necessary for the correct folding of many cell envelope proteins (3). *E. coli* DsbE is a thioredoxin-like protein, involved in cytochrome *c* maturation (4). DsbE has been implicated in the reduction of the thiol ether linkers to the heme of apocytochrome *c* (5), prior to heme ligation by CcmF and CcmH (4, 6). *E. coli* DsbD is a cytoplasmic transmembrane protein responsible for maintaining DsbE in its reduced state in the periplasm (7). *E. coli* DsbC is a homodimer with disulfide bond isomerase activity that is also kept reduced by the transmembrane protein DsbD (8, 9). In contrast, *E. coli* DsbA is a monomer that catalyzes the oxidation of reduced, unfolded proteins (10, 11). DsbA is reoxidized by the transmembrane protein DsbB, which is in turn oxidized by components of the electron transport pathway (12, 13). Dsb proteins, in particular DsbA, have been shown to be involved in virulence in toxin-secreting Gram-negative bacteria such as *Vibrio cholerae* (14, 15), *Yersinia pestis* (16), *Shigella* sp. (17), and *E. coli* (18).

Gram-positive bacteria do not have a periplasm, and proteins that are secreted from the cytoplasm are either cell wall-associated or extracellular. In *Mycobacterium tuberculosis*, the only Dsb proteins present are homologs to *E. coli* DsbE (*Mtb* DsbE or Rv2878c, also known as MPT53) and its redox, transmembrane protein partner, *E. coli* DsbD (*Mtb* DsbD or Rv2874), which are depicted in Fig. 1b. The presence of Dsb proteins in Gram-positive bacteria, such as *M. tuberculosis*, suggests that these proteins are necessary for the correct folding of cell wall-associated and extracellular secreted proteins. Hence, studies of *Mtb* DsbE may give some insights into the virulence of mycobacteria.

*M. tuberculosis* is a pathogenic bacterium that is responsible for tuberculosis, which is the world's leading cause of adult death by a bacterial infectious disease, with 3 million deaths and 10 million new cases per year (19, 20). The *M. tuberculosis* Structural Genomics Consortium is an international effort focusing on determining protein structures from *M. tuberculosis*, including potential drug targets (21, 22). A promising group of

\* This work was supported by Grant NIH 20298-001-01 from the National Institutes of Health, Department of Energy-BER, and Howard Hughes Medical Institute (to D. E.). The costs of publication of this article were defrayed in part by the payment of page charges. This article must therefore be hereby marked "advertisement" in accordance with 18 U.S.C. Section 1734 solely to indicate this fact.

The atomic coordinates and structure factors (code 1LU4) have been deposited in the Protein Data Bank, Research Collaboratory for Structural Bioinformatics, Rutgers University, New Brunswick, NJ (<http://www.rcsb.org/>).

¶ Supported by Deutsche Akademie der Naturforscher Leopoldina Grant BMBF-LPD 9901/8-79.

\*\* Supported by National Institutes of Health Grant GM646222.

§§ To whom correspondence and reprint requests should be addressed: Howard Hughes Medical Institute and UCLA-DOE Institute of Genomics and Proteomics, P.O. Box 951570, Los Angeles, CA 90095-1570. E-mail: david@mbi.ucla.edu.

<sup>1</sup> The abbreviations used are: Dsb, disulfide bond-forming proteins; *Mtb*, *Mycobacterium tuberculosis*; Rv number, Sanger center notation for each gene in *Mtb*.

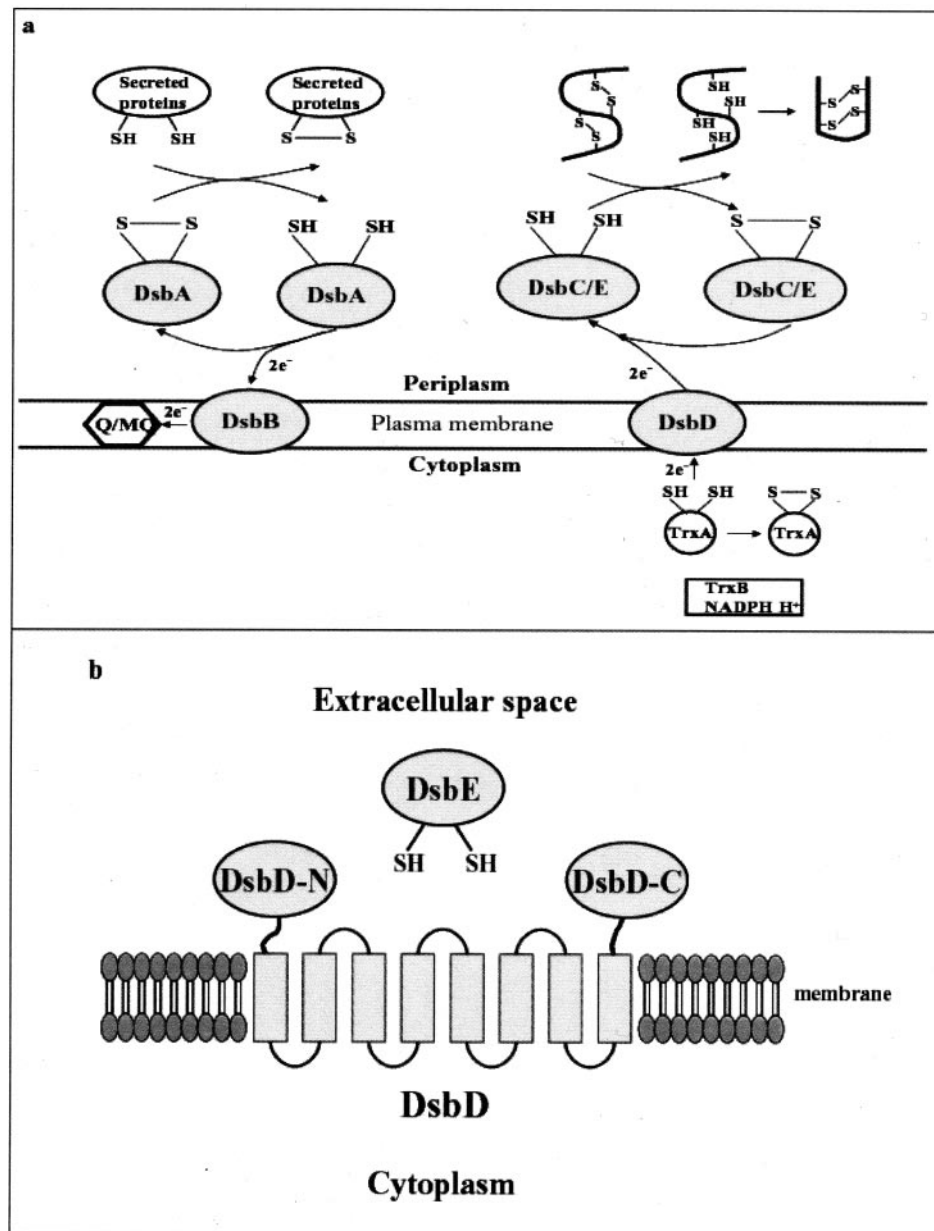


FIG. 1. Model for disulfide bond formation and rearrangement catalyzed by Dsb proteins of *E. coli* (a) and *M. tuberculosis* (b). a, known Dsb proteins in the *E. coli* (Gram-negative bacteria) system. DsbA oxidizes disulfide bonds of newly translocated proteins. The transmembrane protein DsbB accepts electrons from DsbA and transfers them to quinone (Q) or menaquinones (MQ) embedded in the bilayer. DsbC is a disulfide isomerase protein that catalyzes the reformation of incorrectly formed disulfide bonds. DsbE is thought to reduce the cysteines of apocytochrome *c* for heme attachment and is anchored to the inner membrane. These two proteins accept electrons from the cytoplasm (generated from NADPH, thioredoxin (TrxA), and thioredoxin reductase (TrxB)) through the DsbD transmembrane protein. The Dsb proteins all reside in the periplasm of Gram-negative bacteria. b, model of proposed Dsb proteins in the *M. tuberculosis* (Gram-positive bacteria) system. The Dsb protein homologous to the *E. coli* Dsb system found in *M. tuberculosis* reside in the extracellular space (i.e. these proteins are secreted from the bacterial cell wall into the extracellular space). *Mtb* DsbE, which is homologous to *E. coli* DsbE protein, has a cleavable signal peptide. *Mtb* DsbD (Rv2874) is homologous to the *E. coli* DsbD transmembrane protein, which has two predicted soluble domains on the N and C termini of the protein that are connected by eight "predicted" transmembrane helices.

potential drug targets is the secreted proteins of *M. tuberculosis*, which are important in the induction and escape from host immune responses and virulence. *Mtb* DsbE is one such uncharacterized secreted protein. This work presents an example of protein structural analysis leading to functional information.

#### EXPERIMENTAL PROCEDURES

**Purification and Crystallization**—A recombinant plasmid producing the mature DsbE (without the signal peptide, residues 30–159) in pQE30 (Qiagen) was constructed as described previously (23). The purification of *Mtb* DsbE has been previously described (24). The purified protein was dialyzed into 0.5 M NaCl and 0.1 M Tris-HCl, pH 7.4, for crystallization trials. The protein crystallized in 2.2 M NH<sub>4</sub>SO<sub>4</sub>, 5%

isopropyl alcohol, 20% glycerol; the crystals were mounted; and diffraction data were collected under cryoconditions identical to the crystallization conditions. The selenomethionine *Mtb* DsbE protein was prepared as previously described (25) and crystallized under identical conditions to the native protein.

**Data Collection and Structure Determination and Refinement**—A selenomethionine-substituted *Mtb* DsbE crystal diffracted to 1.5 Å, and a native crystal diffracted to 1.1 Å, both having unit cell dimensions of 60.7 × 60.7 × 80.0 Å with one monomer per asymmetric unit in space group P4<sub>3</sub>2<sub>1</sub>2. Data were processed using DENZO and SCALEPACK (26) and multiwavelength anomalous diffraction phasing proceeded by the usual methods of heavy atom location (SHELXD, available on the World Wide Web at shelx.uni-ac.gwdg.de/SHELX/), maximum likelihood phase refinement (27), and density modification (28). Phase extension

TABLE I

X-ray diffraction data collection and atomic refinement for disulfide oxidoreductase DsbE protein from *M. tuberculosis*

The final column refers to the native protein and the preceding columns to the selenomethionine analog.

	Peak	Inflection	High remote	Native
Data set				
Wavelength (Å)	0.978680	0.978437	0.971139	0.978680
Resolution range (Å)	1.5	100–1.5	100–1.5	100–1.1
Unique reflections (total)	45,334 (285,221)	45,355 (248,185)	45,276 (404,618)	57,039 (476,787)
Completeness (%) <sup>a</sup>	99.9 (100.0)	99.8 (99.9)	99.8 (100.0)	99.0 (99.5)
$R_{\text{merge}}^{a,b}$	8.8 (45.7)	8.7 (45.2)	9.2 (45.0)	7.4 (38.2)
$I/\sigma^a$	21.0 (3.2)	19.2 (3.1)	24.0 (4.76)	28.2 (5.11)
No. of selenium sites/monomer	2			
Phasing resolution range (Å)				
$R_{\text{cullis}}^{c,d}$	48.2–1.5	48.2–1.5	48.2–1.5	
Accentric		0.89/0.65	0.78/0.83	
Centric		0.83	0.69	
Figure of merit <sup>e</sup>	0.496/0.881 <sup>f</sup>			
Model refinement				
Resolution range (Å)	20–1.1			
No. of reflections (working/free)	54102/2840			
No. of protein atoms	1018			
No. of water molecules	313			
$R_{\text{work}}/R_{\text{free}}^g$ (%)	14.3/20.3			
Root mean square deviations				
Bond lengths (Å)	0.020			
Bond angles (degrees)	1.713			

<sup>a</sup> Statistics for the highest resolution shell are given in parentheses.<sup>b</sup>  $R_{\text{merge}} = \sum |I - \langle I \rangle| / \sum I$ .<sup>c</sup> The inflection data set was treated as a reference for phasing.<sup>d</sup>  $R_{\text{cullis}} = \sum \epsilon / \sum |F_{\text{PH}} - F_{\text{P}}|$ , where  $\epsilon$  = lack of closure.<sup>e</sup> Value is given after density modification.<sup>f</sup> After density modification.<sup>g</sup>  $R_{\text{work}} = \sum |F_{\text{obs}} - F_{\text{calc}}| / \sum F_{\text{obs}}$ .  $R_{\text{free}}$  was computed identically except where all reflections belong to a test set of 5% randomly selected data.

to 1.1 Å permitted automated model building for all but five residues of the protein with ARP/WARP (29) and was refined using SHELXL. Model building was done in O (30), and the final model includes all 134 residues of the monomer. Data and refinement statistics are shown in Table I.

**Structure and Sequence Analysis**—BLAST and ClustalW were used for data base searches and multiple sequence alignments, respectively. Pairwise alignments were calculated by the Smith-Waterman algorithm. Similar protein structures were searched for using DALI (31) and aligned with combinatorial extension (32). Electrostatic and surface area calculations were performed with WebLabViewer.

**Oxidation and Reduction of *Mtb* DsbE**—To oxidize *Mtb* DsbE, 10 mM GSSG was added to *Mtb* DsbE in 0.5 M NaCl and 0.1 M Tris-HCl, pH 7.4, and incubated for 1 h at room temperature. The oxidized protein was then isolated by gel filtration in its original buffer. To reduce *Mtb* DsbE, 100 mM dithiothreitol was added to *Mtb* DsbE in 0.5 M NaCl and 0.1 M Tris-HCl, pH 7.4, and incubated overnight at 4 °C. The reduced protein was then isolated by gel filtration in its original buffer. To ensure total reduction or oxidation, samples of the treated *Mtb* DsbE were run on an SDS-PAGE gel with no dithiothreitol present, because oxidized samples migrate faster than reduced samples under nonreducing conditions.

**Redox Properties of *Mtb* DsbE: Comparison with Glutathione**—The *in vitro* redox state of *Mtb* DsbE was assayed as described (33, 34). In this assay, the change in fluorescence intensity (excitation wavelength 280 nm) was measured at the wavelength of maximum emission (356 nm for *Mtb* DsbE). Experiments were carried out in 100 mM sodium phosphate, pH 7.0, and 1.0 mM EDTA. Oxidized and reduced *Mtb* DsbE were incubated at 25 °C in the presence of 0.1 mM GSSG and varying concentrations of GSH (0–10 mM) for 12 h before recording the fluorescence emission on a Spex Fluorolog (Jubin Yvon-Spex). The equilibrium concentrations of GSH and GSSG were calculated according to Equations 1–3,

$$[\text{GSH}] = [\text{GSH}]_0 - 2R[\text{DsbE}]_0 \quad (\text{Eq. 1})$$

$$[\text{GSSG}] = [\text{GSSG}]_0 - R[\text{DsbE}]_0 \quad (\text{Eq. 2})$$

$$R = (F - F_{\text{ox}}) / (F_{\text{red}} - F_{\text{ox}}) \quad (\text{Eq. 3})$$

where  $[\text{GSH}]_0$  and  $[\text{GSSG}]_0$  represent the initial concentrations of GSH and GSSG,  $R$  is the relative amount of reduced protein at equilibrium,  $[\text{DsbE}]_0$  is the initial concentration of *Mtb* DsbE in the oxidized form,  $F$  is the fluorescence intensity, and  $F_{\text{ox}}$  and  $F_{\text{red}}$  are the fluorescence intensities of completely oxidized and reduced protein. The equilibrium

constant  $K_{\text{eq}}$  was estimated from nonlinear regression analysis of the data according to the Nernst equation (Equation 4).

$$R = ([\text{GSH}]^2 / [\text{GSSG}]) / (K_{\text{eq}} + [\text{GSH}]^2 / [\text{GSSG}]) \quad (\text{Eq. 4})$$

From the equilibrium constant and by using the glutathione standard potential ( $E'_0_{\text{GSH/GSSG}} = -240$  mV) (35), the standard redox potential ( $E'_0$ ) was calculated with Equation 5.

$$E'_0 = E'_0_{\text{GSH/GSSG}} - \frac{RT}{nF} \ln K_{\text{eq}} \quad (\text{Eq. 5})$$

in which  $F$  represents Faraday's constant,  $n$  is the number of electrons transferred, and  $RT$  is the product of the gas constant and the absolute temperature.

**Redox Properties of *Mtb* DsbE: Comparison with Disulfide Bond Isomerase Protein, DsbC**—The redox potential of *Mtb* DsbE was determined by the method of protein-protein redox equilibria developed by Aslund (35), as modified by Collet and Bardwell (36). The protein used as a standard was *E. coli* DsbC, which has a redox potential ( $E'_0$ ) of  $-135$  mV (37). In short, equimolar amounts of oxidized DsbC and reduced *Mtb* DsbE were incubated in 50 mM Tris/HCl, pH 7.5, 350 mM NaCl, 5 mM EDTA at 25 °C. After different time points, samples were analyzed by reverse phase high pressure liquid chromatography (2695 separations module; Waters). The oxidized and reduced forms of each protein were separated on a Phenomenex Primesphere 5- $\mu\text{m}$  C8 column (buffer A: 0.1% trifluoroacetic acid in water; buffer B: 30% methanol, 60% acetonitrile, 0.1% trifluoroacetic acid). Separation of oxidized and reduced forms of DsbC and *Mtb* DsbE was achieved using a linear gradient from 53 to 62% B over 450 min at a flow rate of 1 ml/min. For evaluation of the redox potential, peak areas were analyzed using PeakFit (Systat), and the redox potential was calculated as described previously (35).

**Determination of  $pK_a$  of *Cys*<sup>36</sup>**—The pH-dependent ionization of the *Cys*<sup>36</sup> thiol (solvent-exposed) was followed by the specific absorbance of the thiolate anion at 240 nm as described earlier (9). As a control, the pH-dependent absorbance for the oxidized form of *Mtb* DsbE was recorded. To avoid precipitation artifacts and to minimize buffer absorbance, a buffer system consisting of 10 mM  $\text{K}_2\text{PO}_4$ , 10 mM boric acid, 10 mM sodium succinate, 1 mM EDTA, and 200 mM KCl (containing 100  $\mu\text{M}$  dithiothreitol for the reduced protein) was used. The pH (initial value of 8.5) was lowered to 2.2 by the stepwise addition of aliquots of 0.1 M HCl, and the absorbance at 240 and 280 nm was recorded and corrected for

the volume increase. Samples had an average initial protein concentration of  $\sim 30 \mu\text{M}$ . The pH dependence of the thiolate-specific absorbance signal ( $S = (A_{240}/A_{280})_{\text{reduced}}/(A_{240}/A_{280})_{\text{oxidized}}$ ) was fitted according to the Henderson-Hasselbalch equation (Equation 6), in which  $S_{\text{AH}}$  represents the corrected absorption intensity of the fully protonated form, and  $S_{\text{A}^-}$  is that of the fully deprotonated form.

$$S = S_{\text{AH}}(S_{\text{A}^-} - S_{\text{AH}})/(1 + 10^{(\text{pK}_a + \text{pH})}) \quad (\text{Eq. 6})$$

**Determination of Unfolding/Folding Equilibrium**—The reversible guanidine hydrochloride (GdnHCl)-induced unfolding/folding of *Mtb* DsbE was performed by measuring the CD ellipticities at 222 nm (38). The spectrum of the reduced form was recorded in the presence of 0.5 mM dithiothreitol. For unfolding equilibrium, *Mtb* DsbE (final concentration of  $7 \mu\text{M}$ ) was dissolved in difference concentrations of GdnHCl and incubated for 3 h at 25 °C. Data were analyzed according to the two-state assumption (39, 40). The standard changes of folding free energy were calculated according to Equation 7.

$$\Delta G_{\text{fold}}^0 = -RT \ln K_{\text{eq}} \quad (\text{Eq. 7})$$

The difference in stability between the oxidized and reduced forms of DsbE protein was calculated as in Equation 8.

$$\Delta \Delta G_{\text{fold}} = \Delta G_{\text{fold,ox}}^0 - \Delta G_{\text{fold,red}}^0 \quad (\text{Eq. 8})$$

**Oxidase activity of *Mtb* DsbE: Refolding of Hirudin**—*Hirudo medicinalis* hirudin (Sigma) refolding was performed as described (41). Reduced, unfolded hirudin ( $28 \mu\text{M}$ ) was incubated with  $84 \mu\text{M}$  oxidized *Mtb* DsbE in 100 mM sodium phosphate, pH 7.0, 1 mM EDTA at 25 °C. At different time points, 100- $\mu\text{l}$  samples were removed, and the reaction was quenched by the addition of 20  $\mu\text{l}$  of formic acid and 20  $\mu\text{l}$  of acetonitrile, respectively. The samples were then analyzed using a Phenomenex Primesphere 5- $\mu\text{m}$  C18 column using a gradient from 30 to 37% D with 0.1% trifluoroacetic acid over 70 min at a flow rate of 1 ml/min. Buffer C was 0.1% trifluoroacetic acid in an aqueous solution, and buffer D was 0.1% trifluoroacetic acid in 80% acetonitrile. Peaks were detected using the Waters W474 fluorescence detector with 274-nm excitation and 325-nm emission wavelength settings.

## RESULTS

**Overall Structure of *Mtb* DsbE**—The crystal structure of *Mtb* DsbE consists of a main domain that contains a thioredoxin fold, with its distinct structural motif consisting of a four-stranded  $\beta$ -sheet made up of  $\beta_3$ ,  $\beta_4$ ,  $\beta_6$ , and  $\beta_7$  and three flanking  $\alpha$ -helices corresponding to  $\alpha_3$ ,  $\alpha_5$ , and  $\alpha_6$  (Fig. 2a). In addition to the thioredoxin fold domain, a short  $3_{10}$ -helix ( $\alpha_1$ ), two  $\beta$ -strands ( $\beta_1$  and  $\beta_2$ ), and another short  $3_{10}$ -helix ( $\alpha_2$ ) appear at the N terminus. A long  $\alpha$ -helix ( $\alpha_4$ ) and a  $\beta$ -strand ( $\beta_5$ ) (forming a five-stranded  $\beta$ -sheet) are found after the  $\beta_3$ - $\alpha_3$ - $\beta_4$  motif of the thioredoxin fold.

**Active Site Dithiols**—The two active site cysteines, Cys<sup>36</sup> and Cys<sup>39</sup>, are reduced as determined by the  $3.69 \pm 0.30 \text{ \AA}$  distance between the two S $\gamma$  atoms (Fig. 2b). A disulfide bond linking the two residues would be expected to have a distance of  $2.03 \pm 0.25 \text{ \AA}$  between the two S $\gamma$  atoms (42). The cysteines adopt a right-handed hook confirmation at the N terminus of helix  $\alpha_3$ , which is consistent for the active site cysteines in the thioredoxin superfamily fold. Only the S $\gamma$  atom of Cys<sup>36</sup> in the dithiol is exposed on the protein surface, whereas S $\gamma$  of Cys<sup>39</sup> is buried, which is usual for a thioredoxin superfamily protein. The sulfur atom of Cys<sup>36</sup> is stabilized by hydrogen bonds to the O $\epsilon$ 1 atom of Gln<sup>100</sup> (3.05  $\text{\AA}$ ) and to the amide nitrogen atom of Pro<sup>37</sup> (3.34  $\text{\AA}$ ) and the amide nitrogen atom of Phe<sup>38</sup> (3.35  $\text{\AA}$ ); the S $\gamma$  atom of Cys<sup>39</sup> is not in a hydrogen-bonding network but does have a hydrophobic interaction with conserved cis-Pro<sup>101</sup> (4.15  $\text{\AA}$ ) as does Cys<sup>36</sup>.

**Crystallographic Dimeric Contacts**—There is a crystallographic homodimeric interface that could possibly be in the transient heterodimer interface for oxidoreductase activity, especially since the interface is in the vicinity of the CXXC active site region. The surface area of each monomer is 6400  $\text{\AA}^2$ , and the buried surface area of each monomer at the interface is 600

$\text{\AA}^2$ , which is  $\sim 10\%$  of the total surface area and corresponds to a transient homodimeric interface (43). A  $\pi$ -cation interaction occurs between the aromatic ring of Trp<sup>35'</sup> and the active site, Cys<sup>36</sup> (the prime on position 35' indicates that this residue is on the neighboring molecule). Arg<sup>64</sup> from one monomer buries itself into the other monomer, forming hydrogen bonds with symmetry-related residues. The NH1 and NH2 atoms of Arg<sup>64</sup> both hydrogen-bond to atom N $\epsilon$ 1 of Trp<sup>99'</sup> and the oxygen atom of Asn<sup>117'</sup> respectively, via a water molecule, and both hydrogen-bond to the oxygen atom of Gln<sup>100'</sup>. Furthermore, the N $\epsilon$  atom of Arg<sup>64</sup> interacts with the oxygen atom of Pro<sup>118'</sup>. Other notable homodimer interface hydrogen bonds are atom N $\epsilon$ 1 of Trp<sup>99</sup> to atoms O $\epsilon$ 1 of Gln<sup>100'</sup> and to the oxygen atom of both Val<sup>97'</sup> and Pro<sup>98'</sup>. There are also hydrophobic interactions seen between the rings of Trp<sup>99</sup> and Trp<sup>92'</sup>.

**Structural Comparisons**—The known structure with the highest structural similarity to *Mtb* DsbE is *Bradyrhizobium japonicum* CcmG/DsbE (*B. japonicum* DsbE) (44), a Gram-negative bacterial DsbE periplasmic protein. The alignment of the two structures gives a root mean square deviation over backbone atoms of 1.8  $\text{\AA}$ . The structure with the second highest similarity is *B. japonicum* TlpA (45), which is involved in the maturation of cytochrome *aa*<sub>3</sub> (root mean square deviation of 2.1  $\text{\AA}$ ). Fig. 3, a–c, shows the structural similarity between the three proteins, *Mtb* DsbE, *B. japonicum* DsbE, and *B. japonicum* TlpA, respectively. The most obvious difference between these three proteins is that the active site cysteines in the *B. japonicum* DsbE and *B. japonicum* TlpA structures are in their oxidized states but are in their reduced states in the *Mtb* DsbE structure.

**Gram-positive *Mtb* DsbE Protein Functions Differently from Gram-negative DsbE Proteins**—The function of DsbE homologs in Gram-positive bacteria has not previously been characterized. A phylogenetic tree derived from prokaryotic homologs to *E. coli* DsbE shows that the Gram-positive and Gram-negative DsbE homolog proteins cluster into two groups with the extremophile *Deinococcus radiodurans* separating the two groups (data not shown). The divergence of Gram-negative and Gram-positive DsbE homologs and the difference in redox state of *Mtb* DsbE and *B. japonicum* DsbE crystal structures suggest that Gram-positive DsbE and Gram-negative DsbE homologs may function differently.

**Determination of the Redox Potential of *Mtb* DsbE**—To further characterize *Mtb* DsbE, the redox potential relative to that of glutathione was determined, which compares the ability of reduced glutathione to transfer electrons to a protein. The  $K_{\text{eq}}$  of *Mtb* DsbE is  $\sim 0.25 \pm 0.2 \text{ mM}$  (Fig. 4a). The corresponding standard redox potential ( $E'_0$ ) calculated for *Mtb* DsbE is  $-128 \pm 12 \text{ mV}$ . In comparison with the standard redox potential for *E. coli* DsbA ( $-124 \text{ mV}$ ) (46), which is an oxidant, and *E. coli* thioredoxin ( $-269 \text{ mV}$ ) (35), which is a reductant, the standard redox potential for *Mtb* DsbE ( $-128 \text{ mV}$ ) suggests that DsbE is an oxidant. In contrast, the standard redox potentials for Gram-negative DsbE proteins ( $-217$  to  $-175 \text{ mV}$ ) (47–49) correspond to these proteins being weak reductants. Since *Mtb* DsbE is an oxidant and Gram-negative DsbE proteins are weak reductants, this reinforces the hypothesis that Gram-negative and Gram-positive DsbE proteins function differently.

To confirm the redox potential that was determined by equilibrium incubation using GSH/GSSG as a reference, we applied a method based on the analysis of the direct protein-protein redox equilibrium between *Mtb* DsbE and the protein *E. coli* DsbC, which has a well established redox potential of  $E'_0$  is  $-135 \text{ mV}$  (37). By analyzing the equilibrium between *E. coli* DsbC and *Mtb* DsbE, we determined the redox potential of *Mtb*

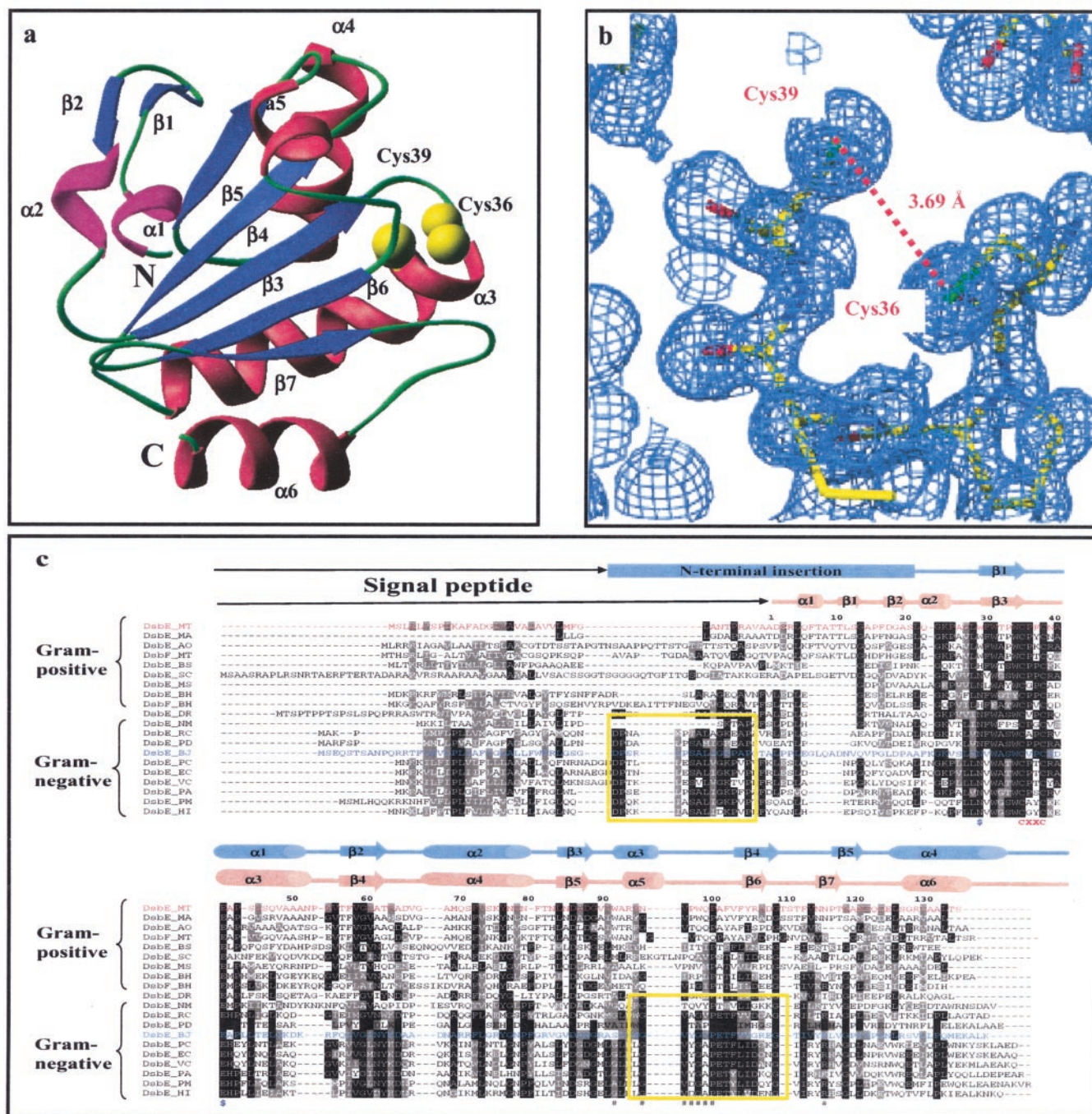


**FIG. 2. Three-dimensional structure of *Mtb* DsbE and sequence comparisons of DsbE homologs.** *a*, ribbon diagram of the monomer.  $\alpha$ -Helices,  $3_{10}$ -helices, and  $\beta$ -strands are shown in red, purple, and blue, respectively. The active site Cys sulfur atoms and  $\beta$ -carbon atoms are shown in yellow. This image was generated using RIBBONS. *b*, The *Mtb* DsbE active site; a view of the final  $2F_o - F_c$  electron density map at the active site region. The electron density is contoured at 1.2 $\sigma$ . The distance between the two Cys sulfur atoms is 3.69 Å. This image was generated using RIBBONS. *c*, sequence comparison of DsbE homologs. The first and second diagrams depict the *B. japonicum* DsbE monomer (blue; sequence also in blue) and the *Mtb* DsbE monomer (red; sequence also in red) in terms of secondary structure elements, respectively. Residues labeled with a number sign have two distinct conformations in the *Mtb* DsbE structure. Residues with a dollar sign are the residues that form a hydrogen bond between  $\alpha$ -helix 3 and  $\beta$ -strand 3. The sequence alignment of DsbE homologs was made with ClustalW. The DsbE proteins cluster into two main groups, Gram-negative bacteria and Gram-positive bacteria, with the extremophile (*D. radiodurans*) separating the two groups. The yellow boxes show blocks of conserved residues in the Gram-negative bacterium that are not seen in Gram-positive bacterium. *MT*, *M. tuberculosis*; *MA*, *Mycobacterium avium*; *AO*, *Amycolatopsis orientalis*; *BS*, *Bacillus subtilis*; *SC*, *Streptomyces coelicolor*; *MS*, *Mycobacterium smegmatis*; *BH*, *Bacillus halodurans*; *DR*, *D. radiodurans*; *NM*, *Neisseria meningitidis*; *RC*, *Rhodobacter capsulatum*; *PD*, *Paracoccus denitrificans*; *BJ*, *B. japonicum*; *PC*, *Pantoea citrea*; *EC*, *E. coli*; *VC*, *V. cholerae*; *PA*, *Pseudomonas aeruginosa*; *PM*, *Pasteurella multocida*; *HI*, *Hemophilus influenzae*.

DsbE ( $E'_0$ ) to be  $-128 \pm 3$  mV. This is in very good accordance with the value determined using GSH/GSSG as a reference. This makes *Mtb* DsbE one of the most oxidizing proteins known.

**Determination of the  $pK_a$  Value of *Mtb* DsbE**—Determination of the  $pK_a$  value of the *Mtb* DsbE solvent-exposed active

site cysteine provides further evidence that *Mtb* DsbE is functionally divergent from Gram-negative DsbE proteins. The  $pK_a$  value of the active site cysteine of *Mtb* DsbE (Cys<sup>36</sup>) was measured by observing the change in absorption of the cysteines at 240 nm over a pH range of pH 2–9 (Fig. 4b). The  $pK_a$  value of the solvent-exposed active site cysteine

FIG. 3. **Ribbon diagrams of *Mtb* DsbE and two of the proteins with similar structures.** *a-c*, ribbon diagrams of the structures with the active site cysteines indicated with an arrow. These images were generated using RIBBONS. *a*, *Mtb* DsbE; *b*, *B. japonicum* DsbE; *c*, *B. japonicum* TlpA. It should be noted that all three structures have similar topology, although in *Mtb* DsbE the active site is in its reduced form, whereas in *B. japonicum* DsbE and *B. japonicum* TlpA the active sites are in their oxidized form.

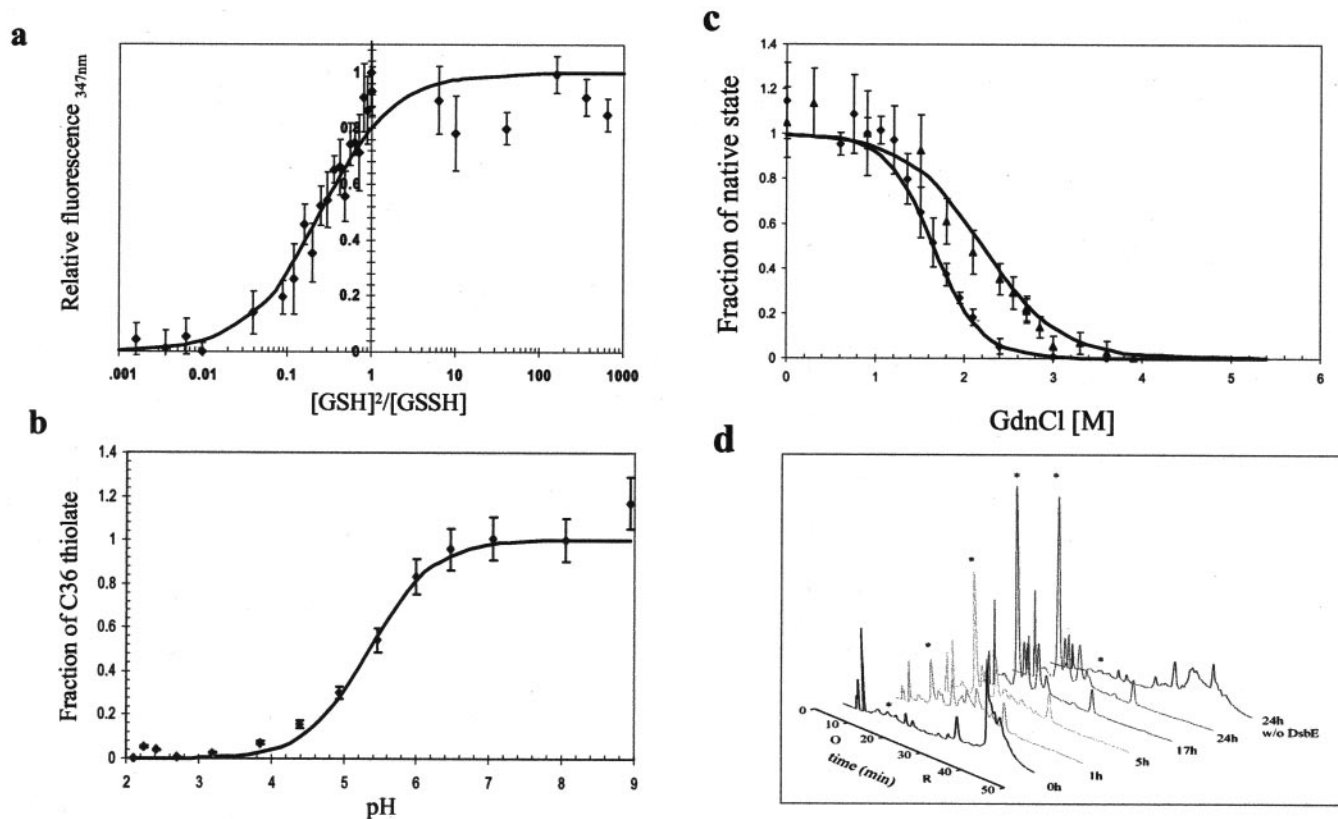
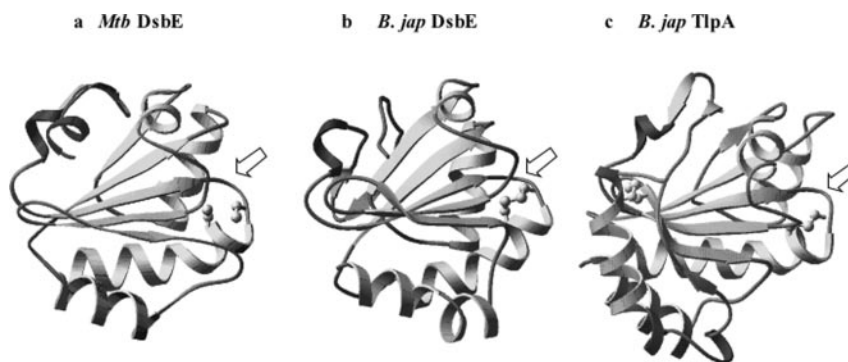


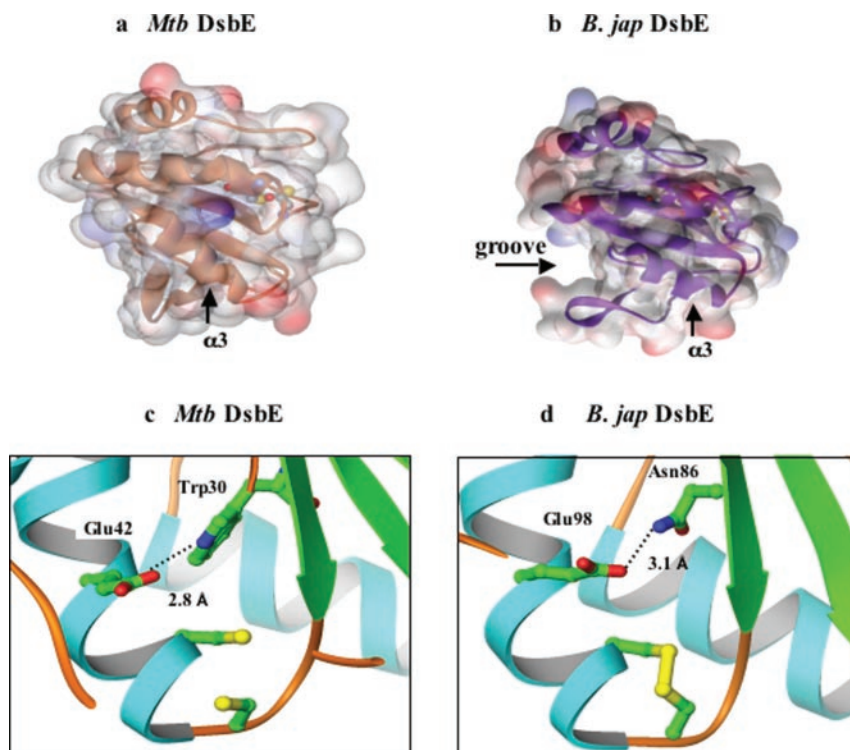
FIG. 4. **Biochemical Characterization of *Mtb* DsbE.** *a*, redox equilibrium of *Mtb* DsbE with glutathione. The y axis represents the proportion of *Mtb* DsbE present in the reduced form at equilibrium with various mixtures of reduced (GSH) and oxidized (GSSG) glutathione (x axis), which was measured by exploiting the difference in fluorescence (347 nm) of reduced *Mtb* DsbE compared with oxidized *Mtb* DsbE. Equilibrium concentrations of oxidized and reduced *Mtb* DsbE and GSH and GSSG were calculated as described (33, 34). The equilibrium constant was calculated to be  $0.25 \pm 0.2$  mM, which is consistent with *Mtb* DsbE acting as an oxidant. *b*, determination of the  $pK_a$  values of the active site cysteine, Cys<sup>36</sup>, in *Mtb* DsbE. The absorption specific to reduced *Mtb* DsbE protein is shown as a function of pH (x axis) compared with the fraction of Cys<sup>36</sup> thiolate (y axis). The  $pK_a$  value of Cys<sup>36</sup> was calculated by fitting the data points as described in Ref. 9. The  $pK_a$  of Cys<sup>36</sup> in *Mtb* DsbE is  $5.0 \pm 0.2$ . *c*, GdnHCl-dependent unfolding/folding of *Mtb* DsbE. GdnHCl-dependent unfolding was monitored by circular dichroism spectroscopy at 222 nm of oxidized *Mtb* DsbE (shown as diamonds) and reduced *Mtb* DsbE (shown as triangles). Refolding of oxidized *Mtb* DsbE is shown by open diamonds, and refolding of reduced *Mtb* DsbE is shown by open triangles. GdnHCl concentration is the x axis, and the y axis represents the fraction of native (folded) protein. Since the reduced form of *Mtb* DsbE unfolds at higher concentrations of GdnHCl than the oxidized form, the reduced form of *Mtb* DsbE is its more stable form. *d*, analysis of the refolding kinetics of reduced and unfolded hirudin. A 3-fold molar excess of oxidized *Mtb* DsbE was used and incubated with reduced unfolded hirudin at pH 7.0 and 25 °C. Samples were removed as indicated on each time course and quenched as described. The peak for the oxidized hirudin is marked by an asterisk. O and R mark the retention time for oxidized and reduced hirudin, respectively. The rightmost trace is after a 24-h incubation in the absence of *Mtb* DsbE (w/o DsbE).

(Cys<sup>36</sup>) is  $5.0 \pm 0.2$ . This is relatively acidic compared with the solvent-exposed active site cysteine of *E. coli* thioredoxin ( $pK_a$  of 7.5) (50) and *E. coli*  $\Delta 57$ DsbE ( $pK_a$  of 6.8) (47) and that of reduced glutathione ( $pK_a$  of 8.7), although not as acidic as *E. coli* DsbA, which is a known oxidant whose  $pK_a$  of the solvent-exposed active site cysteine is 3.5 (51). The acidic nature of the solvent-exposed Cys<sup>36</sup> provides further evidence that *Mtb* DsbE has different biochemical characteristics than its Gram-negative DsbE homologs.

**Thermodynamic Properties of the Redox Forms**—To compare

stabilities of the different redox forms of *Mtb* DsbE, guanidine hydrochloride-induced unfolding and refolding of both oxidized and reduced forms was examined by circular dichroism. The reduced form of *Mtb* DsbE is more stable than that of the oxidized form, given that the reduced form of the protein denatures at a higher concentration of guanidine hydrochloride than the oxidized form (Fig. 4c). Calculation of the free energy change ( $\Delta\Delta G_{\text{redox}}$ ) between the reduced and oxidized form of *Mtb* DsbE suggests that the reduced form is  $12.4 \pm 4$  kJ/mol more stable than the oxidized form. *E. coli* DsbA (an oxidant) is

**FIG. 5. Molecular surface representation of monomeric and active site of *Mtb* DsbE and *B. japonicum* DsbE.** *a*, illustration of the transparent molecular surface of *Mtb* DsbE with the ribbon diagram of the structure in orange. *b*, illustration of the transparent molecular surface of *B. japonicum* DsbE with the ribbon diagram of the structure in purple. The potential protein interaction groove is indicated. Helix  $\alpha_3$  is labeled in both structures. The figure shows that there is no potential protein interaction groove seen in the *Mtb* DsbE structure as compared with the *B. japonicum* DsbE structure. *c* and *d*, ribbon diagrams of the active sites of *Mtb* and *B. japonicum* DsbE structures. The  $\alpha$ -helices and  $\beta$ -strands are shown in cyan and green, respectively. The active site cysteines and amino acid pair atoms are shown in green, red, blue, and yellow, representing carbon, oxygen, nitrogen, and sulfur, respectively. These images were generated using RIBBONS. *c*, *Mtb* DsbE; *d*, *B. japonicum* DsbE. The hydrogen bond between Trp<sup>30</sup> and Glu<sup>42</sup> in the *Mtb* DsbE structure maintains a conformation in which the active cysteines are in their reduced form. In contrast, the hydrogen bond between Asn<sup>86</sup> and Glu<sup>98</sup> in the *B. japonicum* DsbE structure maintains a conformation that allows a disulfide bond to form between the active site cysteines.



also more stable in its reduced form, with a  $\Delta\Delta G_{\text{redox}}$  of  $16.3 \pm 3.6$  kJ/mol (41), whereas *E. coli* thioredoxin (a reductant) is  $16.3 \pm 2.4$  kJ/mol more stable in its oxidized form (52). Thus, the increased stability of *Mtb* DsbE in its reduced form is consistent with *Mtb* DsbE being energetically more stable as an oxidant.

**Oxidase Activity of *Mtb* DsbE and Hirudin Refolding**—In order to investigate the oxidative protein folding ability of *Mtb* DsbE, we tested its ability to oxidize hirudin from *H. medicinalis*. Hirudin is a 6.9-kDa protein that functions as an inhibitor of thrombin. It contains three intramolecular disulfide bridges that connect residues 6–14, 16–28, and 22–39. The regeneration of native recombinant hirudin from the reduced unfolded form to the fully oxidized native state was carried out in the presence and absence of *Mtb* DsbE in stoichiometric quantities. In the absence of added *Mtb* DsbE, a small quantity of spontaneous (presumably air-mediated) oxidation of hirudin occurred to generate randomly oxidized hirudin, as has previously been observed, but negligible native hirudin was generated (Fig. 4d). In contrast, *Mtb* DsbE was able to oxidize hirudin from a denatured reduced state to a completely folded and oxidized state (Fig. 4d). This shows that *Mtb* DsbE is capable of oxidizing substrate proteins.

#### DISCUSSION

**Comparison of *Mtb* DsbE with Gram-negative DsbE Homologs**—Several lines of evidence imply that *Mtb* DsbE does not function in the same way as its Gram-negative homologs. DsbE proteins in Gram-negative bacteria have been shown to be weak reductants, whose solvent-exposed active site cysteines have  $pK_a$  values around 6.5–6.8. We have shown that *Mtb* DsbE is an oxidant, and its solvent-exposed, active site cysteine has a lower  $pK_a$  (5.0) than those of Gram-negative bacterial DsbE homologs. These differences and the observation that the sequences of Gram-positive DsbE homologs cluster together imply that Gram-positive DsbE proteins, and in particular *Mtb* DsbE, have a different biochemical function than Gram-negative DsbE homologs.

Sequence and structural alignments of Gram-negative and Gram-positive DsbE homologs also suggest different functions. They show two regions that are conserved among Gram-negative DsbE homologs but are significantly different in Gram-positive DsbE proteins (Fig. 2c, yellow boxes). The first N-terminal region, conserved in the Gram-negative DsbE homologs contains an insertion of 15 residues that are absent in the *Mtb* DsbE structure (Fig. 2c). The additional 15 residues, together with alterations in surrounding residues, generate a region that is structurally similar to a  $\beta$ -hairpin. This region forms a distinct groove on the protein's molecular surface (Fig. 5b), which has been shown to have the required architecture for interaction with the protein partners of *B. japonicum* DsbE (44). Sequence alignments show that this region is well conserved among Gram-negative DsbE proteins (Fig. 2c, N-terminal yellow box). In contrast, the *Mtb* DsbE has a shorter N-terminal region, the  $3_{10}$ - $\beta$ - $3_{10}$  segment (Fig. 2c), which does not form a groove on the protein's molecular surface (Fig. 5a). This region is poorly conserved among Gram-positive DsbE proteins. Since this groove is thought to play an important role in protein-protein interactions of *B. japonicum* DsbE, we may conjecture that the protein interaction partners of *Mtb* DsbE differ from that of *B. japonicum* DsbE (44), that *Mtb* DsbE does not use this region for protein-protein interactions, or both. A second region of conserved residues in Gram-negative DsbE homologs contains the Gram-negative DsbE protein motif (53),  $^{152}\text{GVXGXPET}^{159}$ , which is located in a solvent-exposed loop region between  $\alpha_3$  and  $\beta_4$  in the *B. japonicum* DsbE structure (Fig. 2c, second yellow box). The side chains of these residues pack tightly around the protein backbone and do not protrude into the solvent. In Gram-positive bacteria, this motif is not conserved, and the corresponding sequence in *Mtb* DsbE,  $^{96}\text{NVPWQPAF}^{103}$ , contains residues that protrude from the protein backbone to form a potential homodimer interface. The *B. japonicum* DsbE crystal structure contains no crystallographic or potential homodimer interface (44). In summary, the differences in the sequence conservation between the Gram-

negative DsbE proteins and Gram-positive DsbE proteins reinforce our conclusion that *Mtb* DsbE functions differently from Gram-negative DsbE proteins.

Comparison of the active sites of *B. japonicum* DsbE and *Mtb* DsbE structures is also consistent with the hypothesis that Gram-negative and Gram-positive homologs of DsbE function differently. *B. japonicum* DsbE crystallized in its oxidized form, and *Mtb* DsbE crystallized in its reduced form (Fig. 3, *b* and *a*, respectively), suggesting that the active site environment differs between the two proteins. The active site of *B. japonicum* DsbE is unusually acidic, due to residues Asp<sup>97</sup>, Glu<sup>98</sup>, and Glu<sup>158</sup> (which are conserved among the Gram-negative DsbE proteins), which may account for the reducing power of *B. japonicum* DsbE compared with *Mtb* DsbE. The corresponding residues in *Mtb* DsbE (Ala<sup>41</sup>, Glu<sup>42</sup>, and Ala<sup>102</sup>) are not acidic except for Glu<sup>42</sup>, which is conserved throughout the DsbE homologs (Fig. 2*c*). Alignment of the two structures in the vicinity of the active site loop (residues Trp<sup>30</sup>–Glu<sup>42</sup> and Asn<sup>86</sup>–Glu<sup>98</sup> in the *Mtb* DsbE and *B. japonicum* DsbE, respectively) gives a root mean square deviation over backbone atoms of 0.42 Å (Fig. 5, *c* and *d*). Thus, the redox state of DsbE proteins is not dependent on a conformational change near the active site, implying that the redox state of the protein is not determined by the architecture of the active site.

Structural analysis implicates an amino acid pair that contributes to the stability of the reduced and oxidized forms of the Dsb proteins. In the reduced form of *Mtb* DsbE, the amino acid pair Trp<sup>30</sup> and Glu<sup>42</sup> are flanking the active site residues in  $\beta$ -strand 3 ( $\beta$ 3) and  $\alpha$ -helix 3 ( $\alpha$ 3), respectively (Fig. 5*c*), and form hydrogen bonds between N $\epsilon$ 1 of Trp<sup>30</sup> and both O $\epsilon$ 1 and O $\epsilon$ 2 of Glu<sup>42</sup> (2.90 and 2.77 Å). This interaction probably contributes to the stability of the active site loop to form a conformation where the reduced thiol form of the active site cysteines is favored, and therefore *Mtb* DsbE is an oxidant. This amino acid pair is well conserved throughout the Gram-positive DsbE proteins. In comparison, within the *B. japonicum* DsbE structure (44), which crystallized in its oxidized form, the corresponding residues are Asn<sup>86</sup> and Glu<sup>98</sup>. These two residues also form a hydrogen bond (3.08 Å) across the  $\beta$ -strand and  $\alpha$ -helix (Fig. 5*d*), possibly maintaining the active site loop in a conformation that favors the disulfide form of the active site cysteines. In all of the Dsb and thioredoxin structures determined thus far, there is a corresponding conserved amino acid pair that forms a hydrogen bond between the  $\beta$ -strand and  $\alpha$ -helix containing the active site cysteines in the protein's most stable form. For example, the structure of *E. coli* DsbA, an oxidant, shows the amino acid pair to be Glu<sup>37</sup> and Lys<sup>58</sup>. In the reduced form of DsbA (the more stable form), the hydrogen bond between Glu<sup>37</sup> and Lys<sup>58</sup> has a distance of 2.92 Å, whereas in the oxidized form, the distance is  $\sim$ 0.75 Å greater (54). This implies that the hydrogen bonding flanking the active site in thioredoxin-like proteins may influence their redox state by favoring conformations in which active site cysteines are most stable in their reduced or oxidized states.

**Biological Implications**—In Gram-negative bacteria, it has been proposed that DsbE proteins are involved in the maturation of cytochrome *c*. Cytochrome *c* maturation converts a linear polypeptide, the apocytochrome, into a three-dimensional structure that contains one or more covalently bound, redox-active heme co-factors. There are at least three systems of cytochrome *c* maturation of varying complexity (55, 56). Gram-negative bacteria cytochrome *c* maturation utilizes a well characterized pathway, System I, which contains periplasmic anchored DsbE (6, 56). Since Gram-negative DsbE has been proposed to play a role as a reductant, and we have shown that *Mtb* DsbE is an oxidant, the reduction of the cysteines of

apocytochrome *c* would be an unfavorable reaction. This suggests that *Mtb* DsbE is not involved in cytochrome *c* maturation via System I. Cytochrome *c* maturation in Gram-positive bacteria is thought to utilize System II, which is a less well characterized pathway as compared with System I (55, 57). System II also contains a predicted thioredoxin-like protein (Ccs1/ResB), and the *M. tuberculosis* genome contains all of the known genes in System II cytochrome *c* maturation. Thus *Mtb* DsbE may be involved in cytochrome *c* maturation by the System II pathway.

An alternative role for *Mtb* DsbE could be to function as a disulfide bond-forming (Dsb) protein. The *M. tuberculosis* genome contains no genes that encode for other homologs of Dsb proteins, such as *E. coli* DsbA, DsbC, or DsbG. In Gram-negative bacteria, Dsb proteins function in the periplasm. Because *M. tuberculosis* is a Gram-positive bacterium and does not contain a periplasmic space, *Mtb* DsbE might function extracellularly within the cell wall environment. If so, *Mtb* DsbE might function as a disulfide isomerase to ensure that secreted or surface-associated proteins have correctly formed disulfide bonds. It has been predicted that greater than 60% of the 161 predicted secreted proteins of *M. tuberculosis* contain at least one disulfide bond.<sup>2</sup> However, *in vitro*, we found no activity for disulfide bond isomerase in *Mtb* DsbE (data not shown); nor did previous studies (24). Therefore, if *Mtb* DsbE functions as an isomerase, this suggests a high specificity of *Mtb* DsbE for its functional protein partners.

The final option and the one that we favor is that *Mtb* DsbE may have a similar function to *E. coli* DsbA, which catalyzes the oxidation of reduced, unfolded proteins with disulfide bonds (10, 11). This hypothesis is supported by the observation that *Mtb* DsbE and *E. coli* DsbA are both oxidants, and their solvent-exposed active site cysteines both have relatively low  $pK_a$  values, 5.0 and 3.4 (38), respectively. In addition, *Mtb* DsbE has been shown to have oxidase activity as it reoxidizes reduced hirdurin. In fact, the NCBI conserved domain site selects the first 50 residues of *Mtb* DsbE in having a DsbA domain. Therefore, *Mtb* DsbE may catalyze the oxidation and folding of reduced, unfolded proteins as they are secreted into the extracellular space of the *M. tuberculosis* cell wall environment.

In summary, structural and functional analysis of *Mtb* DsbE suggests that it has a similar function to *E. coli* DsbA, which catalyzes the oxidation of reduced, unfolded secreted proteins to form disulfide bonds (10, 11). Hence, *Mtb* DsbE may be involved in virulence, since many secreted proteins may depend on the oxidase activity of *Mtb* DsbE to form correctly folded proteins. Interestingly, although the overall structures of Gram-negative and Gram-positive DsbE proteins have similar thioredoxin-like folds, the structural differences between these two proteins imply that they function differently (the N-terminal regions, the potential interaction interfaces, and the redox state of the active sites differ between the two proteins). Biochemical analysis of *Mtb* DsbE confirms this assumption, since *Mtb* DsbE is an oxidant probably acting upon secreted proteins, whereas *B. japonicum* DsbE is a weak reductant acting upon apocytochrome *c*. Thus, the determination and analysis of the structure of *Mtb* DsbE along with comparison with homologous sequences and structures has provided an opportunity to make specific predictions about protein function that were confirmed biochemically.

**Acknowledgments**—We thank Drs. Michael Sawaya and Duilio Cascio for invaluable help with data collection and general crystallography and Parag Mallick for statistics on disulfide bonds in the *M. tuberculosis* genome. We also thank Brookhaven National Laboratory

<sup>2</sup> P. Mallick, personal communication.

for the use of beamline X8C of the National Synchrotron Light Source, particularly Joel Berendzen, Li Wei Hung, and Leonid Flaks.

## REFERENCES

- Martin, J. L. (1995) *Structure* **3**, 245–250
- Schroder, E., and Ponting, C. P. (1998) *Protein Sci.* **7**, 2465–2468
- Missiakas, D., and Raina, S. (1997) *J. Bacteriol.* **179**, 2465–2471
- Grove, J., Busby, S., and Cole, J. (1996) *Mol. Gen. Genet.* **252**, 332–341
- Reid, E., Cole, J., and Eaves, D. J. (2001) *Biochem. J.* **355**, 51–58
- Fabianek, R. A., Hofer, T., and Thony-Meyer, L. (1999) *Arch. Microbiol.* **171**, 92–100
- Stewart, E. J., Katzen, F., and Beckwith, J. (1999) *EMBO J.* **18**, 5963–5971
- Rietsch, A., Bessette, P., Georgiou, G., and Beckwith, J. (1997) *J. Bacteriol.* **179**, 6602–6608
- Bessette, P. H., Cotto, J. J., Gilbert, H. F., and Georgiou, G. (1999) *J. Biol. Chem.* **274**, 7784–7792
- Bardwell, J. C., McGovern, K., and Beckwith, J. (1991) *Cell* **67**, 581–589
- Joly, J. C., and Swartz, J. R. (1997) *Biochemistry* **36**, 10067–10072
- Missiakas, D., Georgopoulos, C., and Raina, S. (1993) *Proc. Natl. Acad. Sci. U. S. A.* **90**, 7084–7088
- Bader, M., Muse, W., Ballou, D. P., Gassner, C., and Bardwell, J. C. (1999) *Cell* **98**, 217–227
- Hu, S. H., Peek, J. A., Rattigan, E., Taylor, R. K., and Martin, J. L. (1997) *J. Mol. Biol.* **268**, 137–146
- Manning, P. A. (1997) *Gene (Amst.)* **192**, 63–70
- Zav'yalov, V. P., Chernovskaya, T. V., Chapman, D. A., Karlyshev, A. V., MacIntyre, S., Zavalov, A. V., Vasiliev, A. M., Denesyuk, A. I., Zav'yalova, G. A., Dudich, I. V., Korpela, T., and Abramov, V. M. (1997) *Biochem. J.* **324**, 571–578
- Yu, J., and Kroll, J. S. (1999) *Microbes Infect.* **1**, 1221–1228
- Zhang, H. Z., and Donnenberg, M. S. (1996) *Mol. Microbiol.* **21**, 787–797
- Raviglione, M. C., Snider, D., Jr., and Kochi, A. (1995) *JAMA (J. Am. Med. Assoc.)* **273**, 220–226
- Pablos-Mendez, A., Raviglione, M. C., Laszlo, A., Binkin, N., Rieder, H. L., Bustreo, F., Cohn, D. L., Lambregts-van Weezenbeek, C. S., Kim, S. J., Chaulet, P., and Nunn, P. (1998) *N. Engl. J. Med.* **338**, 1641–1649
- Goulding, C. W., Apostol, M., Anderson, D. H., Gill, H. S., Smith, C. V., Kuo, M. R., Yang, J. K., Waldo, G. S., Suh, S. W., Chauhan, R., Kale, A., Bachhawat, N., Mande, S. C., Johnston, J. M., Lott, J. S., Baker, E. N., Arcus, V. L., Leys, D., McLean, K. J., Munro, A. W., Berendzen, J., Sharma, V., Park, M. S., Eisenberg, D., Sacchetti, J., Alber, T., Rupp, B., Jacobs, W., Jr., and Terwilliger, T. C. (2002) *Curr. Drug Targets Infect. Disord.* **2**, 121–141
- Goulding, C. W., Perry, L. J., Anderson, D., Sawaya, M. R., Cascio, D., Apostol, M. I., Chan, S., Parseghian, A., Wang, S., Wu, Y., Cassano, V., Gill, H. S., and Eisenberg, D. (2003) *Biophys. Chem.* **105**, 361–370
- Manca, C., Lyashchenko, K., Wiker, H. G., Usai, D., Colangeli, R., and Gennaro, M. L. (1997) *Infect. Immun.* **65**, 16–23
- Wiker, H. G., Michell, S. L., Hewinson, R. G., Spierings, E., Nagai, S., and Harboe, M. (1999) *Microb. Pathog.* **26**, 207–219
- Van Duynne, G. D., Standaert, R. F., Karplus, P. A., Schreiber, S. L., and Clardy, J. (1993) *J. Mol. Biol.* **229**, 105–124
- Otwinowski, Z., and Minor, W. (1996) *Methods Enzymol.* **276**, 307–326
- Collaborative Computational Project 4 (1994) *Acta Crystallogr. D Biol. Crystallogr.* **50**, 760–763
- Cowtan, K., and Main, P. (1998) *Acta Crystallogr. D Biol. Crystallogr.* **54**, 487–493
- Perrakis, A., Morris, R., and Lamzin, V. S. (1999) *Nat. Struct. Biol.* **6**, 458–463
- Jones, T. A., Zou, J. Y., Cowan, S. W., and Kjeldgaard, M. (1991) *Acta Crystallogr. A* **47**, 110–119
- Holm, L., and Sander, C. (1993) *J. Mol. Biol.* **233**, 123–138
- Shindyalov, I. N., and Bourne, P. E. (1998) *Protein Eng.* **11**, 739–747
- Rossmann, R., Stern, D., Loferer, H., Jacobi, A., Glockshuber, R., and Hennecke, H. (1997) *FEBS Lett.* **406**, 249–254
- Loferer, H., Wunderlich, M., Hennecke, H., and Glockshuber, R. (1995) *J. Biol. Chem.* **270**, 26178–26183
- Aslund, F., Berndt, K. D., and Holmgren, A. (1997) *J. Biol. Chem.* **272**, 30780–30786
- Collet, J. F., Riemer, J., Bader, M. W., and Bardwell, J. C. (2002) *J. Biol. Chem.* **277**, 26886–26892
- Zapun, A., Missiakas, D., Raina, S., and Creighton, T. E. (1995) *Biochemistry* **34**, 5075–5089
- Hennecke, J., Spleiss, C., and Glockshuber, R. (1997) *J. Biol. Chem.* **272**, 189–195
- Santoro, M. M., and Bolen, D. W. (1988) *Biochemistry* **27**, 8063–8068
- Wunderlich, M., Jaenicke, R., and Glockshuber, R. (1993) *J. Mol. Biol.* **233**, 559–566
- Hennecke, J., Sebbel, P., and Glockshuber, R. (1999) *J. Mol. Biol.* **286**, 1197–1215
- Engh, R. A., and Huber, R. (1991) *Acta Crystallogr. A* **47**, 392–400
- Nooren, I. M., and Thornton, J. M. (2003) *J. Mol. Biol.* **325**, 991–1018
- Edeling, M. A., Guddat, L. W., Fabianek, R. A., Thony-Meyer, L., and Martin, J. L. (2002) *Structure* **10**, 973–979
- Capitani, G., Rossmann, R., Sargent, D. F., Grutter, M. G., Richmond, T. J., and Hennecke, H. (2001) *J. Mol. Biol.* **311**, 1037–1048
- Wunderlich, M., and Glockshuber, R. (1993) *Protein Sci.* **2**, 717–726
- Li, Q., Hu, H., and Xu, G. (2001) *Biochem. Biophys. Res. Commun.* **283**, 849–853
- Fabianek, R. A., Huber-Wunderlich, M., Glockshuber, R., Kunzler, P., Hennecke, H., and Thony-Meyer, L. (1997) *J. Biol. Chem.* **272**, 4467–4473
- Setterdahl, A. T., Goldman, B. S., Hirasawa, M., Jacquot, P., Smith, A. J., Kranz, R. G., and Knapp, D. B. (2000) *Biochemistry* **39**, 10172–10176
- Chivers, P. T., Prehoda, K. E., Volkman, B. F., Kim, B. M., Markley, J. L., and Raines, R. T. (1997) *Biochemistry* **36**, 14985–14991
- Grauschopf, U., Winther, J. R., Korber, P., Zander, T., Dallinger, P., and Bardwell, J. C. (1995) *Cell* **83**, 947–955
- Mossner, E., Huber-Wunderlich, M., and Glockshuber, R. (1998) *Protein Sci.* **7**, 1233–1244
- Fabianek, R. A., Hennecke, H., and Thony-Meyer, L. (2000) *FEMS Microbiol. Rev.* **24**, 303–316
- Guddat, L. W., Bardwell, J. C., and Martin, J. L. (1998) *Structure* **6**, 757–767
- Kranz, R., Lill, R., Goldman, B., Bonnard, G., and Merchant, S. (1998) *Mol. Microbiol.* **29**, 383–396
- Thony-Meyer, L. (2002) *Biochem. Soc. Trans.* **30**, 633–638
- Kranz, R. G., Beckett, C. S., and Goldman, B. S. (2002) *Res. Microbiol.* **153**, 1–6